JGR Space Physics

RESEARCH ARTICLE
10.1029/2024JA032575

Statistical Survey of Thin Current Sheets in Earth's Magnetotail: MMS Observations

Zhibo Zhang[1], San Lu[1,2,3], Quanming Lu[1,2,3], Rongsheng Wang[1,2,3], Chenchen Zhan[1], Xinmin Li[1], and Anton V. Artemyev[4,5]

[1]CAS Key Laboratory of Geoscience Environment, School of Earth and Space Sciences, CAS Center for Excellence in Comparative Planetology, University of Science and Technology of China, Hefei, China, [2]Deep Space Exploration Laboratory, Hefei, China, [3]Collaborative Innovation Center of Astronautical Science and Technology, Harbin, China, [4]Department of Earth, Planetary, and Space Sciences, Institute of Geophysics and Planetary Physics, University of California, Los Angeles, CA, USA, [5]Space Research Institute, Moscow, Russia

Key Points:

- We collect a data set of 163 thin current sheet crossing events in Earth's magnetotail using MMS data during 2017–2020
- The thin current sheet has a smaller thickness, a higher current density and a stronger Hall electric field on the duskside than the dawnside
- The Hall electric field in the magnetotail thin current sheet is stronger when the current sheet is thinner

Supporting Information:

Supporting Information may be found in the online version of this article.

Correspondence to:

S. Lu,
lusan@ustc.edu.cn

Citation:

Zhang, Z., Lu, S., Lu, Q., Wang, R., Zhan, C., Li, X., & Artemyev, A. V. (2024). Statistical survey of thin current sheets in Earth's magnetotail: MMS observations. *Journal of Geophysical Research: Space Physics*, *129*, e2024JA032575. https://doi.org/10.1029/2024JA032575

Received 22 FEB 2024
Accepted 8 MAY 2024

Abstract Thin current sheets (TCS) formed in Earth's magnetotail and hosting magnetic field line reconnection are important element of magnetospheric dynamics. In this paper, a statistical survey of 163 TCS crossing events in Earth's magnetotail using observations by MMS during 2017–2020 is performed. We find that magnetotail TCSs typically have a very strong current density primarily carried by electrons, with a thickness of a few ion inertial lengths. Our statistical results reveal different characteristics between TCSs located on the duskside and dawnside. Specifically, we find that TCSs on the duskside have a smaller thickness, higher current density, and stronger Hall electric field than on the dawnside. Our results also show that there is a correlation between the TCS thickness and the Hall electric field magnitude, with a stronger Hall electric field present in thinner TCSs. Our statistics results confirm previously reported key TCS dawn-dusk asymmetries, with the main advance of directly measurable plasma currents. TCS characteristics of the presented data set will be useful for initialization of realistic numerical simulations and theoretical investigations of TCS instabilities resulted in various dynamical models of the magnetotail.

1. Introduction

During the growth phase of a substorm, solar wind energy is transported from the dayside into the nightside and accumulated as magnetic energy, and the magnetotail current sheet thins to form a thin current sheet (TCS), typically with a thickness on the order of ion kinetic scales (McPherron et al., 1973; Sanny et al., 1994). The instability initiated at the TCS facilitates magnetic reconnection, which can release the stored energy in the magnetotail, leading to the acceleration of charged particles and global magnetotail reconfiguration (Genestreti et al., 2023a, 2023b; Q. Lu et al., 2022; S. Lu et al., 2020). As a result, it is generally recognized that the structure and instability of TCSs play a crucial role in the dynamics of magnetospheric substorms (Angelopoulos et al., 2008; Baker et al., 1996; Sitnov, Birn, et al., 2019). Modeling of TCS formation and dynamics require detailed information about their structure (see discussion in Sitnov et al., 2006; Sitnov, Birn, et al., 2019; Zelenyi et al., 2011), and this motivates spacecraft statistical investigations of TCSs.

Since the first direct observation of magnetotail TCS by ISEE-1/2 (Mitchell et al., 1990; Sergeev et al., 1993), there have been numerous efforts to unveil the properties of TCSs through spacecraft observations. The Cluster spacecraft with four-point magnetic field measurements allowed for estimation of the current density profiles along the current sheet normal (Runov et al., 2006). The current sheet thickness was found to be 5 to 10 proton gyroradius calculated in magnetotail lobe field. It was also revealed that the current sheet is almost always embedded in a thicker and weaker background current sheet (or plasma sheet) (Asano et al., 2005; Runov et al., 2006), which differs significantly from the Harris current sheet model (Harris, 1962) typically used for investigations of the magnetic reconnection. This structure is described as an embedded current sheet (or embedded TCS) and the TCS boundary magnetic field was found to be approximately 30%–50% of the lobe magnetic field (Artemyev et al., 2010; Petrukovich et al., 2011), that is, the TCS thickness is about one proton gyroradius calculated in the magnetic field of TCS boundary. The observations also revealed a dawn-dusk asymmetry in the magnetotail TCSs, with a smaller thickness and stronger current density on the duskside (Artemyev et al., 2011; Rong et al., 2011). Another important result is that the current density in the magnetotail TCS is typically up to 10 nA/m^2 and mainly carried by electrons, with almost negligible contribution from protons (e.g., Artemyev et al., 2011; Petrukovich et al., 2015; Runov et al., 2006). Limited by Cluster's near-polar orbit,

the above observations only studied TCSs at a radial distance of ~19 R_E. The even more important limitation of the Cluster-based statistics is the current density measurement technique, the curlometer (Dunlop et al., 2002; Runov, Sergeev, Nakamura, et al., 2005), that averages the current density over the spatial-scale of the spacecraft separations (~1,000 km for main Cluster measurements). The physical process of TCS formation at radial distances closer to the Earth ($X \sim -10$ to -12 R_E) has been investigated using three-point measurements by the Time History of Events and Macroscale Interactions during Substorms (THEMIS) mission (Artemyev, Angelopoulos, Runov, & Petrokovich, 2016), with the same limitations of current density estimates using the curlometer technique. Using single-spacecraft Geotail data collected in 1994–1995, TCSs are also widely present in the middle tail ($X \sim -50$ to -20 R_E) and distant tail ($X \sim -100$ to -80 R_E), with characteristics similar to near-Earth TCSs (Vasko et al., 2015). Additionally, observations have shown that the TCS can extend from inner magnetosphere transition region to the midtail during the growth phase of a substorm, with the entire current sheet responding coherently to external driving forces (Pulkkinen et al., 1999). Single spacecraft measurements of the current density require TCS flapping motion and largely relies on the assumption of uniform velocity of such motion (see discussion in Sergeev et al., 1998, 2006). Contrast to Cluster-based curlometer technique and flapping-based estimates, the Magnetospheric Multiscale mission (MMS; Burch et al., 2016) mission provides a unique opportunity for direct measurements of plasma (ion and electron) currents (see, e.g., S. Lu et al., 2019), and therefore MMS-based statistical investigations of TCS characteristics are important for confirming Cluster, THEMIS, and Geotail results, and for determination of actual (non averaged) current density magnitude.

Recently, the key role of the Hall effect in the magnetotail TCS has been revealed by three-dimensional global hybrid and particle-in-cell simulations (S. Lu et al., 2016, 2018; Pritchett & Lu, 2018). The magnetotail current sheet thinned to the ion kinetic scale driven by an external electric field, and the ions become partially demagnetized while the electrons remain magnetized, leading to the presence of a Hall electric field directed toward the center of the TCS (this mechanism of TCS "charging" has been predicted in Hesse et al. (1998)). The magnetized particles (electrons and a portion of ions) undergo $\mathbf{E} \times \mathbf{B}$ drift dawnward, while the unmagnetized ions move duskward under the effect of the pressure gradient drift and transient ion motion (for details see Artemyev & Zelenyi, 2013). The transport of particles and magnetic flux to the dawnside renders the current sheet on the duskside thinner with a stronger current density and Hall electric field therein. The strong current in magnetotail TCSs, carried mainly by electrons, is also generated by this process.

The MMS provides high-resolution, multi-point measurements that enable detailed investigations of TCS properties. S. Lu et al. (2019) have performed a statistical study of 48 TCSs detected by MMS in 2017 and found the presence of Hall electric fields in the TCSs as expected by simulations. Rogers et al. (2023) found MMS spent more than twice as long in TCSs on the duskside than the dawnside during 2017–2020. However, there has been no more comprehensive statistical investigation of the magnetotail TCS characteristics using MMS.

Leveraging the unique capabilities of MMS, this study aims to conduct a statistical survey of TCS in Earth's magnetotail. This paper is organized as follows: we introduce our data set consisting of 163 TCS crossing events and the methods for obtaining current sheet parameters in Section 2; the statistical results are presented in Section 3; the conclusions and discussion are given in Section 4.

2. Data Set and Methods

In this paper, we use MMS1 data collected in 2017–2020 MMS tail seasons to survey TCS events. The instruments involved in this work are as follows: the Fluxgate Magnetometers (FGM) with resolutions of 0.1 s (Russell et al., 2016; Torbert et al., 2016), the Electric Double Probe (EDP) with resolutions of 0.04 s (Ergun et al., 2016; Lindqvist et al., 2016) and the Fast Plasma Investigation (FPI) with resolutions of 4.5 s (Pollock et al., 2017). The local normal coordinate system **l**, **m**, and **n** for each TCS event is determined following the method used in Runov et al. (2006). The **l** axis (**L** direction) is directed along the maximum variance eigenvector from Minimum Variance Analysis applied to the magnetic field (MVAB; Sonnerup & Scheible, 1998). The **m** axis (**M** direction) is along the current density component perpendicular to **l**, that is, $\mathbf{M} = \mathbf{L} \times [(\mathbf{J}/J) \times \mathbf{L}]$, where **J** is the average current averaged over the current sheet crossing. And the **n** axis (**N** direction) is perpendicular to **l** and **m**, that is, $\mathbf{N} = \mathbf{L} \times \mathbf{M}$.

We select TCS crossing events using the following criteria: (a) the spacecraft crosses or approaches the neutral sheet, that is, with $B_l = 0$; (b) the current density has a large peak, $j > 5$ nA/m^2, to exclude weak or thick current sheet crossings; (c) the average ion flow speed is less than 100 km/s to exclude events that may be associated with

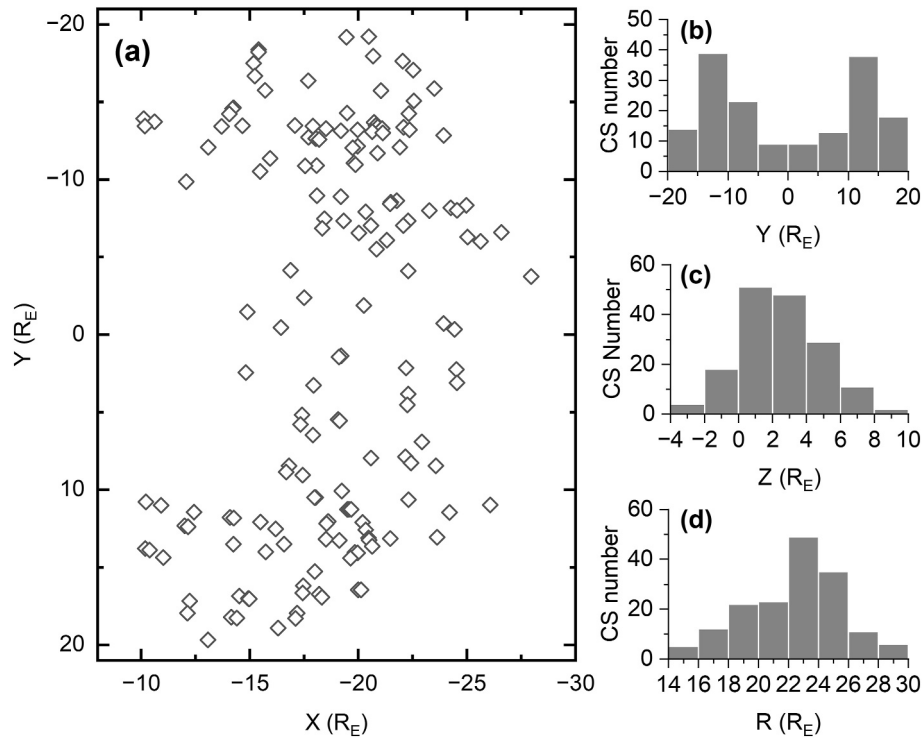

Figure 1. Spatial distribution of the 163 thin current sheets crossing events: (a) in the *XY* plane, (b)–(d) with respect to the coordinate *Y*, *Z* and radial distance *R*.

magnetic reconnection or turbulence; (d) the guide field B_m is not too strong ($<3B_n$) throughout the event to exclude events with strong field-aligned current. We also exclude events with significantly large ion density (>2.0 cm^{-3}), which suggests that these events may be close to cold plasma sheet at the flanks, where magnetosheath plasma may penetrate (Fujimoto et al., 1998). Only events in the magnetotail region ($-30\ R_E < X < -10\ R_E$ and $|Y| < 20\ R_E$, where R_E is Earth's radius) are considered. Using these criteria, we identified a total of 163 TCS crossing events using MMS1 data from 2017 to 2020 (see Table S1 for event list). Note that although our event selecting is restricted intrinsically by the resolution of the FPI data (4.5 s), even the shortest crossing time of our events (~30 s) can be well resolved by FPI, so the selected events meet the necessary requirements for accurate analysis.

Figure 1 shows the spatial distribution of the 163 TCS crossing events. These events were distributed in a large dawn-dusk range from −20 to 20 R_E, with 85 located on the dawnside ($Y < 0$) and 78 on the duskside ($Y > 0$). These events are essentially located at the equatorial plane with the vertical position Z much smaller than X and Y (Figure 1c), so we use $R = \sqrt{X^2 + Y^2}$ as an approximation of the radial distance from Earth. The radial position distribution of events is shown in Figure 1d. The radial distribution of our MMS data set ranges widely from 14 to 30 R_E, whereas Cluster can only measure at a radial distance of ~19 R_E due to its near polar orbit.

In this paper, plasma densities (N_i and N_e), temperatures (T_i and T_e) and electron temperature anisotropy ($T_{e\parallel}/T_{e\perp}$) for each event are average values in the central region of TCS ($|B_l| < 5$ nT). We use particle moments to calculate the current density $\mathbf{j} = eN_e(\mathbf{V}_i - \mathbf{V}_e)$, where e is the electron charge, N_e is the electron number density, and $\mathbf{V}_i$ ($\mathbf{V}_e$) is the ion (electron) velocity. The current density j_0 for each TCS event is the peak value of the current density m-component j_m, and there is no essential currents transverse to $\mathbf{m}$. The magnitude of lobe magnetic field $B_{\rm lobe}$ is evaluated using vertical pressure balance, $B_{lobe} = \sqrt{B_l^2 + 2\mu_0 P_{th}}$, where P_{th} is the thermal pressure. We estimate the TCS thickness using $L_{CS} = B_0/(\mu_0 j_0)$, where B_0 is the magnitude of the magnetic field at the TCS boundary. Because the orbit of MMS is equatorial and the spacecraft often do not reach the TCS boundary, we adopt $B_0 = 0.3B_{\rm lobe}$ based on Cluster statistics (Artemyev et al., 2011).

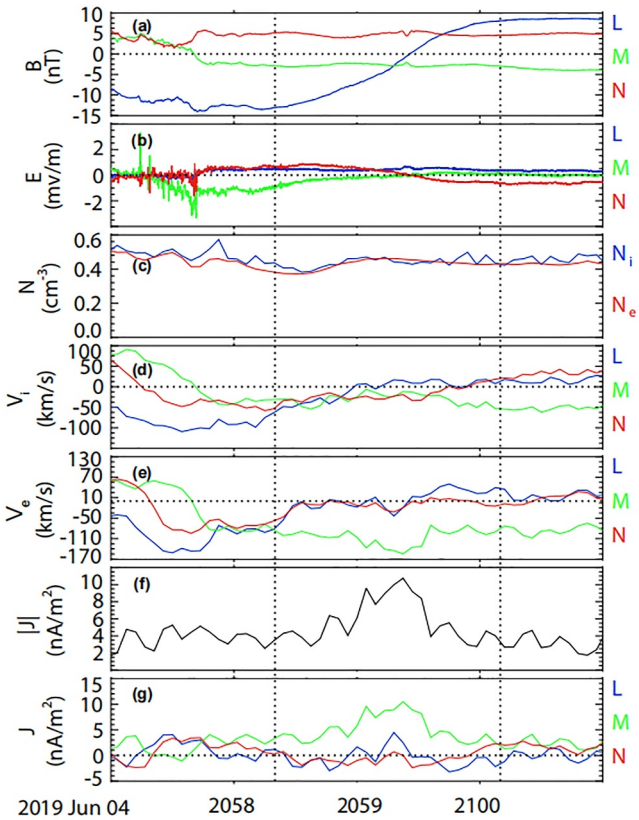

Figure 2. Overview of a typical thin current sheets crossing event observed by MMS1 on 04 June 2019 in LMN coordinates. (a) Magnetic field components. (b) Electric field components. (c) Ion and electron number density. (d) Ion velocity. (e) Electron velocity. (f)–(g) Total current density and current density in three directions from ion and electron moments. The two vertical dotted lines represent the start time and end time of the event.

3. Statistical Results

Figure 2 shows a typical TCS crossing event detected by MMS1 on 04 June 2019, located at [–13.1, −12.1, 3.9] R_E. The magnetic field l-component B_l had a large change from ∼–13 to ∼8 nT and reversed at about 20:59:25 UT (Figure 2a), indicating that the spacecraft crossed current sheet from south to north. The ion flow velocity was small in the entire time period, which indicates that the current sheet was at a quiet time (Figure 2d). A strong current mainly along the **m** direction is seen at the center of the current sheet (Figures 2f and 2g), and the TCS current density $j_0 \approx 10.2$ nA/m^2. The magnitude of lobe magnetic field $B_{\rm lobe} \approx 30.5$ nT. Therefore, the thickness of this current sheet was estimated to be 716 km, which is approximately 2.1 times the local ion inertial length (d_i). Here, d_i is defined as $d_i = \frac{c}{\omega_{pi}} = \sqrt{\frac{m_i c^2}{\mu_0 N_i e^2}}$, where c is the speed of light in vacuum, ω_{pi} is the ion plasma frequency, m_i is the ion mass, μ_0 is the vacuum magnetic permeability, N_i is the ion number density, and e is the elementary charge. In addition, there was a clear polarity change in the electric field n-component E_n from positive to negative, suggesting the presence of the Hall electric field directed toward the center of the TCS (Figure 2b).

Figure 3 presents the distributions of the 163 TCS orientations. The maximum variance MVA eigenvector (**L** direction) located in the geocentric solar magnetospheric coordinate system are shown in Figure 3a. It is evident that the **L** direction primarily points toward the Earth, which corresponds to the configuration of the flaring magnetic lines in Earth's magnetotail. The distribution of the **m**-axis (**M** direction) is shown in Figure 3b. The y-component of the **M** direction is positive for almost all events, indicating that the cross-tail current is generally duskward as expected. Furthermore, the x-component of the **M** direction is negative for 63 out of 78 events on the dawnside, whereas it is positive for 70 out of 85 events on the duskside (Figure 3b). Therefore, the current in the magnetotail current sheet is predominantly perpendicular to the magnetic lines radiating from Earth, flowing from the dawnside to the duskside. We also find that there are numbers of tilted current sheets in the data set, as indicated by the blue arrows in Figure 3b. For most TCSs, the current exhibits a strong vertical component and deviates from the nominal dawn-dusk direction (or the XY plane). This can be attributed to two main reasons, one being a local effect and the other a global or seasonal effect. First, the magnetotail current sheet often undergoes flapping motions, resulting in significant variations in its local normal direction (e.g., Petrukovich et al., 2008; Rong et al., 2010, 2011; Runov, Sergeev, Baumjohann, et al., 2005). Additionally, there is a seasonal effect due to the dipole interaction with the solar wind, which in the summer leads to the current sheet center being at higher Z than the flanks. Figure 3c shows the angle between the **M** direction and the average current direction. The current is not strictly aligned to the **M** direction because there is usually a current component J_l directed toward Earth in the magnetotail TCS because $V_{el} > V_{il}$ (see e.g., S. Lu et al., 2020, 2022). However, J_l is typically much smaller than J_m, so for most events the angle between the **M** direction and the average current direction is sufficiently small (Figure 3c).

Figure 4 shows the characteristics of lobe magnetic field and plasma temperatures using the data set of 163 TCS crossings. Radial profiles of $B_{\rm lobe}$, T_i, and T_e are shown in Figures 4a and 4b, respectively. We use eight 2 R_E wide bins with centers at $R = 15$ R_E to $R = 29$ R_E. Error bars indicate the standard error throughout this paper. It can be seen that the average lobe magnetic field $B_{\rm lobe}$ gradually decreases from ∼42 to ∼21 nT as the distance to Earth increases (Figure 4a). By fitting the lobe magnetic field magnitude as a function of radial distance, we obtained the expression $B_{\rm lobe} \approx 29.8\ {\rm nT} \cdot (R/20\ R_E)^{-0.85}$, which is similar to the results obtained by Shukhtina et al. (2004) for the magnetotail prior to substorm onset. The ion temperature decreases from ∼8 keV in near-Earth events to ∼2 keV in events farther from Earth, while the electron temperature from ∼2.1 to ∼0.3 keV (Figure 4b). A significant number of TCSs (more than 60%) in the data set have temperature ratios $T_i/T_e \sim$ 3–5 (Figure 4c), in agreement with previous observations (Artemyev et al., 2011, 2016b). About 30% events have temperature ratios

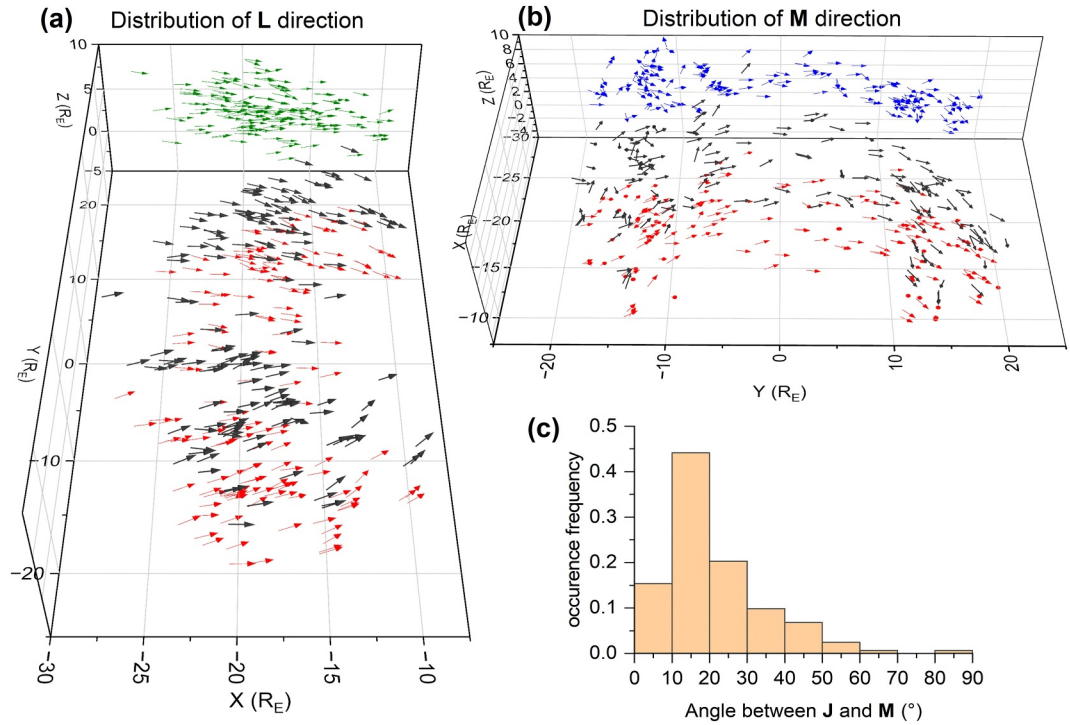

Figure 3. (a and b) Distribution of the **L** direction and the **M** direction of the thin current sheets crossings. The black arrows represent the original vectors in the geocentric solar magnetospheric coordinate system, and the red, green and blue arrows are the projections in the *XY*, *XZ*, and *YZ* planes, respectively. (c) Distribution of the angle between the **M** direction and the average current **J**.

greater than 5. Although electrons in the magnetotail current sheet are generally anisotropic ($T_{e\|}/T_{e\perp} > 1$), the average value of the anisotropy level in our data set is 1.06, with almost all (93%) events having rather weak electronic anisotropy $T_{e\|}/T_{e\perp} < 1.2$ (Figure 4d).

We then study the current density and the thickness of the TCS data set. Figure 5 illustrates the distribution of peak current density j_0 of these 163 events in the *XY* plane. The average value of peak current density is 10.2 nA/m^2, and 73% of events have $j_0 \sim 5$–15 nA/m^2. There are 23 events in the data set with extremely strong current densities ($j_0 > 15$ nA/m^2), 19 of which are located on the duskside. Thus, events with extremely strong currents are more likely to occur on the duskside. Figure 6 shows the distributions of total current density, ion current density and electron current density in the dawn-dusk direction. We use eight 5 R_E wide bins with centers located from $Y = -17.5$ R_E to $Y = 17.5$ R_E. It can be seen that the current density of TCSs has a significant dawn-dusk asymmetry, with stronger current density on the dawnside (especially in the region of $Y \sim 5$–10 R_E). The electron current density is essentially equal to the total current density, while the ion current is very weak, implying that the current carriers are mainly electrons. Figure 7a shows the dawn-dusk distributions of the ion number density N_i and the local ion inertial length d_i. The ion number density varies between 0.4 and 0.6 cm^{-3}, and the local ion inertial length varies between 300 and 400 km. The dawn-dusk distribution of TCS thickness estimated using lobe magnetic field and current density is shown in Figure 7b. The average thickness of these TCS events is about 791 km or 2.3d_i. There is also a clear dawn-dusk asymmetry in the thickness of TCSs, which is smaller on the duskside ($L_{CS} \sim$ 871 km or 2.5d_i) than on the dawnside ($L_{CS} \sim$ 704 km or 2.1d_i).

Finally, we study the Hall electric field in the 163 TCS crossing events. We obtain the Hall electric field using two different methods: (a) using the normal component of the electric field measured directly by the EDP measurements as the Hall electric field; (b) calculating the $\mathbf{E} \times \mathbf{B}$ drift velocity with the magnetic field and plasma measurements to obtain the Hall electric field (for details of the method, see S. Lu et al., 2019; Tsai et al., 2017). Figure 8 shows the vertical profiles of the Hall electric field E_n obtained by two methods, where the horizontal coordinate B_l/B_{lobe} represents the distance from the neutral sheet. Each thin gray curve represents

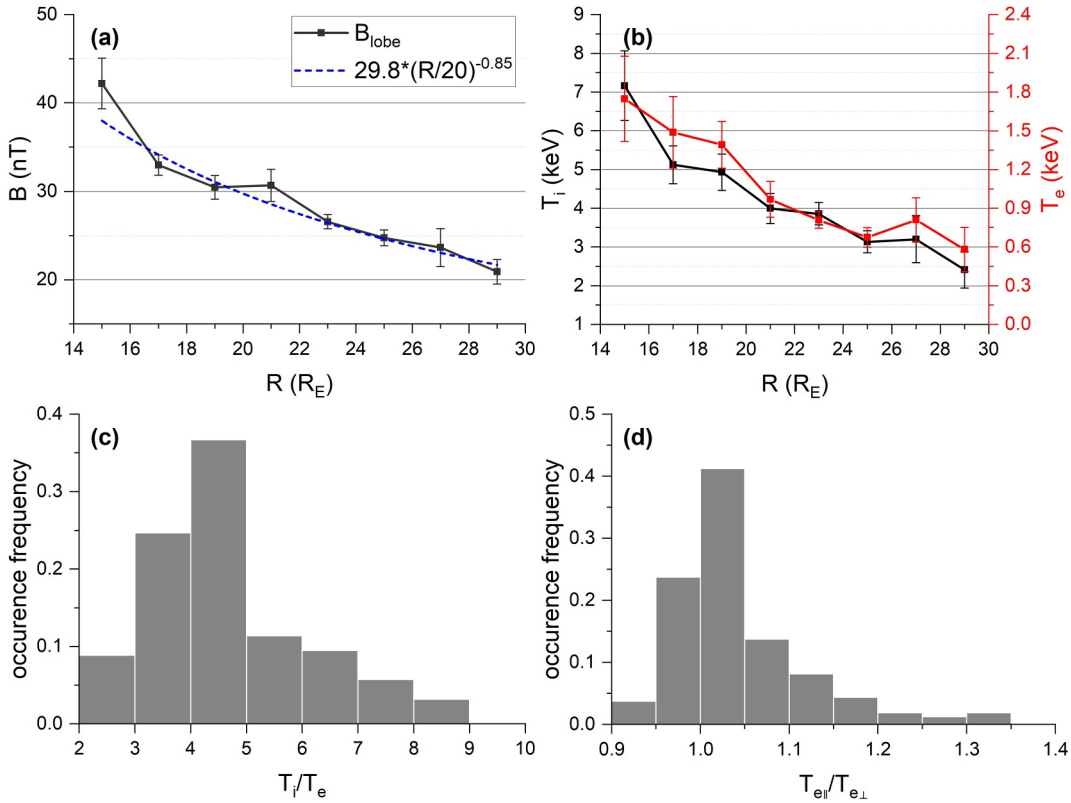

Figure 4. Magnetic field and plasma temperature characteristics in magnetotail TCSs. (a) Radial profiles of B_{lobe}. The dashed blue line is the fitting result. (b) Radial profiles of T_i (black) and T_e (red). (c) Distribution of the temperature ratio T_i/T_e. (d) Distribution of the electron anisotropy $T_{e\|}/T_{e\perp}$.

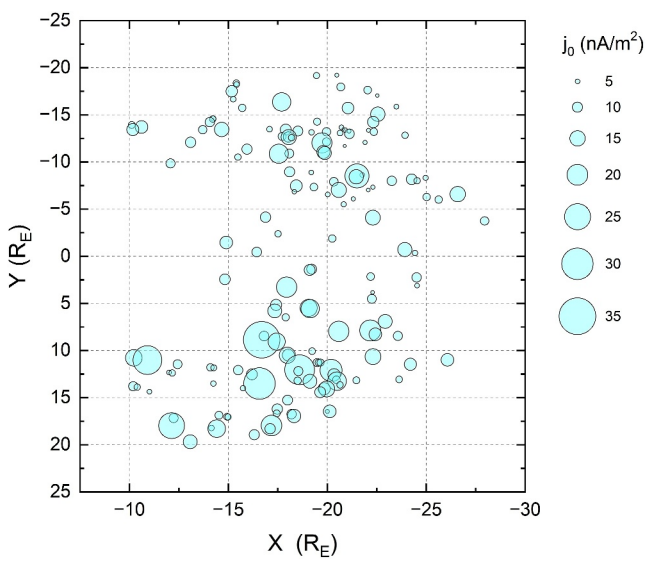

Figure 5. Distribution of the peak current density j_0 in the XY plane. The position of each bubble represents the location of one thin current sheets crossing event, while the radius represents the strength of the current density in this event.

the profile of a single event, and the bold curves represent the averaged profiles. It can be seen that the statistical profiles of the Hall electric field obtained by the two methods are similar, which indicates that the results are reliable. In both methods, the Hall electric field is existing in TCSs and pointing perpendicularly toward the center of the current sheet, which is consistent with previous numerical and theoretical results (e.g., S. Lu et al., 2016, 2018; Pritchett & Coroniti, 1994). The average value of the magnitude of the Hall electric field for the 163 events is about 1 mV/m. Figure 9a shows the dawn-dusk distributions of the magnitude of the Hall electric field obtained by two methods. For each event, we use max(sign $(-B_l)E_n$) as the magnitude of the Hall electric field. The Hall electric field on the duskside is significantly stronger than dawnside, in agreement with the observations by S. Lu et al. (2019). Figure 9b shows the average results of Hall electric field magnitude for events with different current sheet thicknesses, where six $1d_i$-wide bins are used. The average magnitude of the Hall electric field is ~2 mV/m in TCSs thinner than $1d_i$, while the magnitude is ~0.5 mV/m when the thickness is more than $3d_i$. The Hall electric field in the magnetotail TCS tends to be stronger when the current sheet is thinner.

4. Conclusions and Discussion

We have conducted a statistical analysis of 163 thin current sheet crossing events in Earth's magnetotail using MMS data collected in 2017–2020 tail seasons. The main results are as follows:

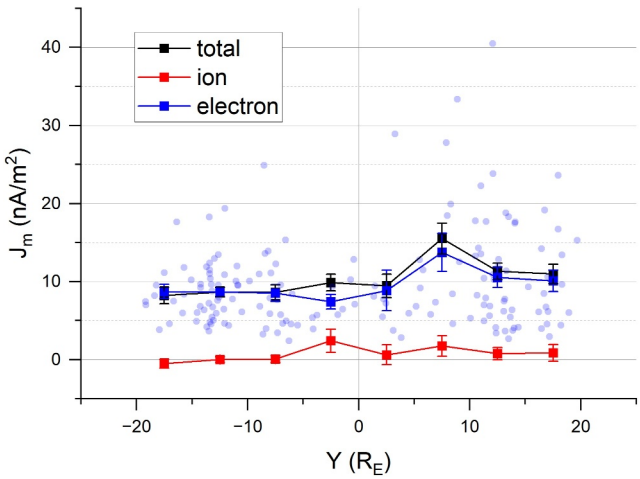

Figure 6. Dawn-dusk distributions of (black) total current density, (red) ion current density, and (blue) electron current density in the thin current sheets crossing events. The blue dots represent the electron current actual observations for each event.

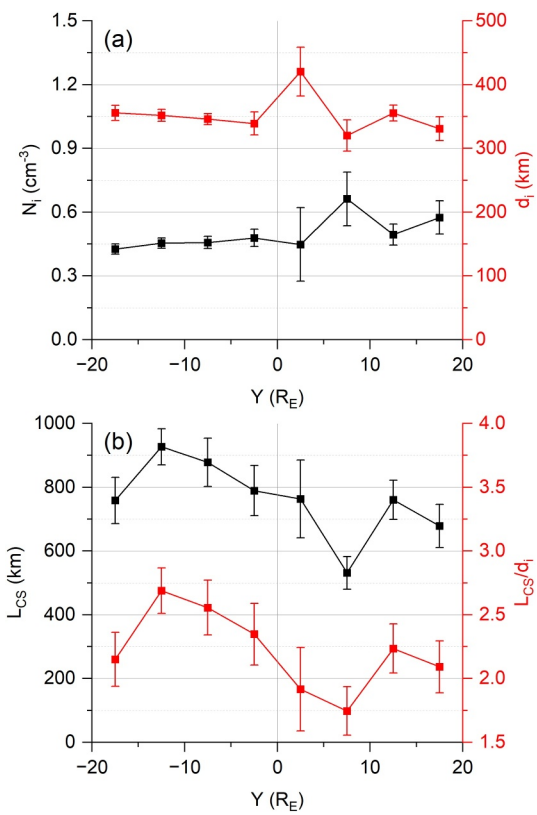

Figure 7. Dawn-dusk distribution of (a) the ion number density (black) and the ion inertial length (red); (b) the current sheet thickness L_{CS} in units of kilometers (black) and in units of ion inertial lengths (red).

1. The current in the magnetotail TCSs is predominantly perpendicular to the magnetic lines radiating from Earth, flowing duskward, and usually has a strong vertical component.
2. The magnitude of the lobe magnetic field in the magnetotail TCSs as a function of radial distance can be expressed by $B_{\text{lobe}} \approx 29.8\ \text{nT} \cdot (R/20\ R_E)^{-0.85}$. The temperature ratio for most TCSs is about 3–5, and the electron temperature anisotropy is weak, mostly less than 1.1.
3. The magnetotail TCSs have a strong current density primarily carried by electrons, typically between 5 and 15 nA/m^2. The thickness of the TCSs is on the ion kinetic scale, typically between 500 and 1,000 km.
4. The magnitude of the Hall electric field in TCSs is approximately 1 mV/m. The Hall electric field tends to be stronger when the current sheet is thinner.
5. There is a significant dawn-dusk asymmetry in the TCS parameters. Compared to the dawnside, the TCS thickness is smaller, the current density is higher, and the Hall electric field is stronger on the duskside. Events with extremely strong currents are occur predominantly on the duskside.

The presence of the Hall electric field in Earth's magnetotail TCS has been proven in previous work by S. Lu et al. (2019), who suggested that the measurements error of electric field is negligible only when the electric field magnitude is up to several millivolts per meter, and thus they indirectly obtained the Hall electric field from magnetic field and plasma measurements following the method used in Tsai et al. (2017). In this paper, in addition to using their method, we also attempted the directly measured electric field to investigate the properties of the Hall electric field in TCSs. As shown in Figure 8, the average profiles of the Hall electric field obtained by the two methods are very similar. Furthermore, although small oscillations occur in direct measurements, the two Hall electric field profiles are roughly coincided for most events. The similarity suggests that the direct measurements of the Hall electric field by MMS are reliable, at least for large sample size statistics. In addition, the reliability of the method used in Tsai et al. (2017) and S. Lu et al. (2019) is also verified, in which it was assumed that the electron flow in the dawn-dusk direction in the magnetotail TCSs is mainly composed of three components: $\mathbf{E} \times \mathbf{B}$ drift velocity, anisotropy drift velocity, and diamagnetic drift velocity.

The Hall electric field has also been detected in the diffusion region of magnetic reconnection (e.g., Eastwood et al., 2007; Øieroset et al., 2001). During magnetic reconnection, the thickness of the reconnection layer is $\lambda_{ez} = \left[\frac{2m_e T_e}{e^2(\partial B_x/\partial z)^2}\right]^{\frac{1}{4}}$ (e.g., Biskamp, 1971; Hesse et al., 1999), which is even thinner than the TCS. Therefore, almost all ions are unmagnetized, and such strong Hall effect causes a large Hall electric field of about 25 mV/m in magnetic reconnection (e.g., Borg et al., 2005; Eastwood et al., 2010). This contrasts with the weaker Hall effect in the TCS, which has a Hall electric field of a few mV/m, due to the fact that the ions are only partially demagnetized.

Thanks to the large radial distribution of the MMS TCS data set, we can study the radial features of the magnetotail TCSs. In this paper, we have studied the variation of the lobe magnetic field and plasma temperatures in TCSs versus the radial distance from Earth. An important issue for magnetotail TCSs is the mechanism of radial (or horizontal) pressure balance (see discussion in

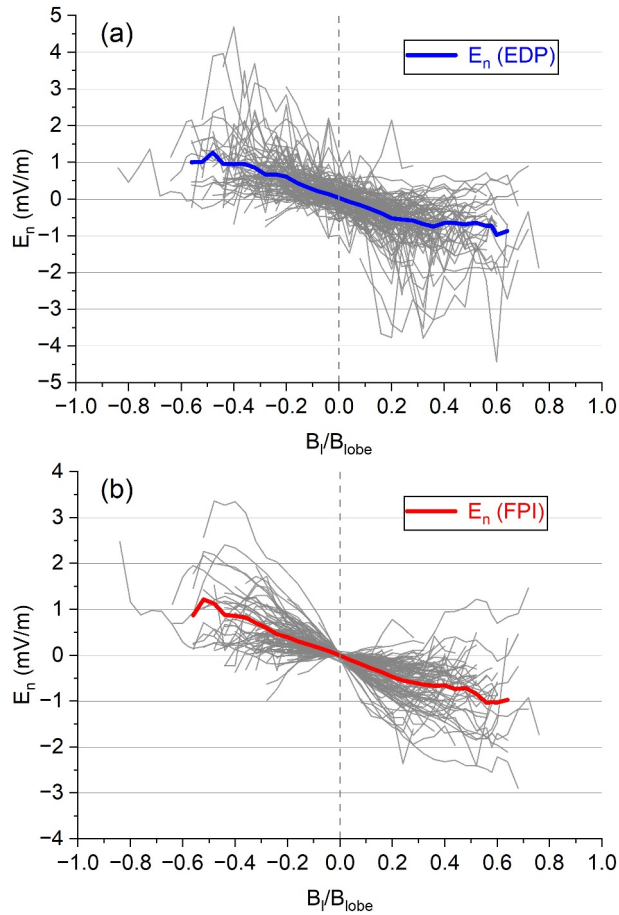

Figure 8. Profiles of the Hall electric field E_n versus B_l/B_{lobe} obtained by two methods: (a) Hall electric field measured directly by Electric Double Probe (EDP) measurements, E_n(EDP), (b) Hall electric field calculated indirectly from FGM and Fast Plasma Investigation (FPI) measurements, E_n(FPI).

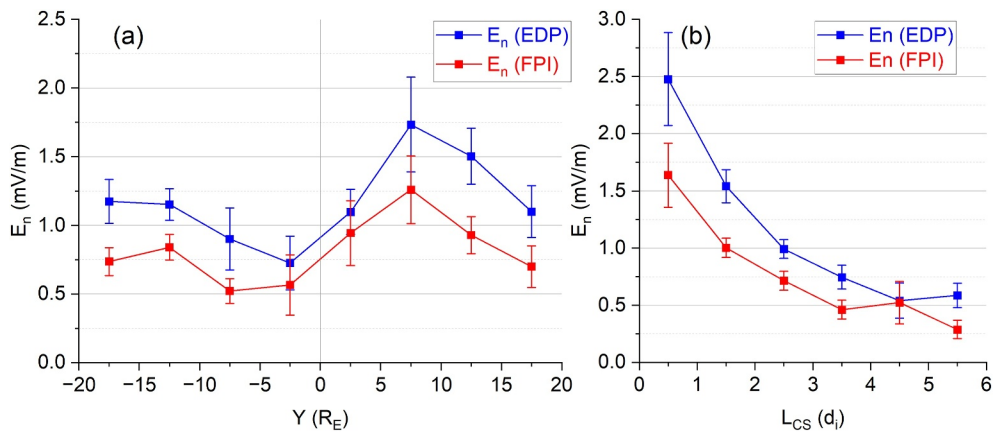

Figure 9. Statistics of the magnitude of the Hall electric field obtained by two methods, direct Electric Double Probe (EDP) measurements, E_n(EDP), and calculated indirectly from FGM and Fast Plasma Investigation (FPI) measurements, E_n(FPI). Distributions (a) in the dawn-dusk direction, and (b) versus current sheet thickness.

Artemyev, Angelopoulos, & Runov, 2016; Sitnov & Merkin, 2016; Sitnov, Stephens, et al., 2019). In widespread class of isotropic TCS models (see, e.g., Baumjohann et al., 2007 ; Yoon & Lui, 2005 and references therein), the horizontal pressure balance can be described by the equation $j_y B_z = \partial p/\partial x$, that is, the magnetic tension force $j_y B_z$ is balanced by the plasma pressure gradient $\partial p/\partial x$ (Rich et al., 1972). Our observations show that TCSs typically have a strong current density up to 10 nA/m^2, which would lead to the formation of a very strong magnetic tension force. However, it is unlikely that the plasma pressure gradient is strong enough to balance this force, and it is suggested that the key contribution of ion nongyrotropy (P_{xz}) should be considered (An et al., 2022; Arnold & Sitnov, 2023; Artemyev et al., 2021; Artemyev, Angelopoulos, & Runov, 2016; Runov et al., 2021; Sitnov & Arnold, 2022). This nongyrotropy is expected to be contributed by hot ion population, likely outside the FPI energy range (see discussion in Arnold & Sitnov, 2023; Artemyev et al., 2019). With the Hot Plasma Composition Analyzers (HPCA; Young et al., 2016) of MMS, the contribution of the ion nongyrotropy to the pressure balance can be investigated in the future.

Data Availability Statement

All the MMS data using in this work can be downloaded at the MMS data center (https://lasp.colorado.edu/mms/sdc/). For data access and processing, the software SPEDAS V4.1 (Version 4.1) (Angelopoulos et al., 2019) was used, which is available at the page https://spedas.org/.

Acknowledgments
This work was supported by National Natural Science Foundation of China Grants 42274196 and 42174181, National Key Research and Development Program of China (No. 2022YFA1604600), and the Strategic Priority Research Program of Chinese Academy of Sciences, Grants XDB 41000000 and XDB0560000. We are thankful to the entire MMS team and instrument principal investigators for providing and calibrating data.

References

An, X., Artemyev, A., Angelopoulos, V., Runov, A., Lu, S., & Pritchett, P. (2022). Configuration of magnetotail current sheet prior to magnetic reconnection onset. *Geophysical Research Letters*, *49*(6), e2022GL097870. https://doi.org/10.1029/2022GL097870

Angelopoulos, V., Cruce, P., Drozdov, A., Grimes, E. W., Hatzigeorgiu, N., King, D. A., et al. (2019). The space physics environment data analysis system (SPEDAS) (version 4.1). [Software]. *Space Science Reviews*, *215*(1), 9. https://doi.org/10.1007/s11214-018-0576-4

Angelopoulos, V., McFadden, J. P., Larson, D., Carlson, C. W., Mende, S. B., Frey, H., et al. (2008). Tail reconnection triggering substorm onset. *Science*, *321*(5891), 931–935. https://doi.org/10.1126/science.1160495

Arnold, H., & Sitnov, M. I. (2023). PIC simulations of overstretched ion-scale current sheets in the magnetotail. *Geophysical Research Letters*, *50*(15), e2023GL104534. https://doi.org/10.1029/2023GL104534

Artemyev, A., Lu, S., El-Alaoui, M., Lin, Y., Angelopoulos, V., Zhang, X.-J., et al. (2021). Configuration of the Earth's magnetotail current sheet. *Geophysical Research Letters*, *48*(6), e2020GL092153. https://doi.org/10.1029/2020GL092153

Artemyev, A., & Zelenyi, L. (2013). Kinetic structure of current sheets in the Earth magnetotail. *Space Science Reviews*, *178*(2), 419–440. https://doi.org/10.1007/s11214-012-9954-5

Artemyev, A. V., Angelopoulos, V., & Runov, A. (2016). On the radial force balance in the quiet time magnetotail current sheet. *Journal of Geophysical Research: Space Physics*, *121*(5), 4017–4026. https://doi.org/10.1002/2016JA022480

Artemyev, A. V., Angelopoulos, V., Runov, A., & Petrokovich, A. A. (2016). Properties of current sheet thinning at $x \sim -10$ to $-12\ R_E$. *Journal of Geophysical Research: Space Physics*, *121*(7), 6718–6731. https://doi.org/10.1002/2016JA022779

Artemyev, A. V., Angelopoulos, V., Vasko, I. Y., Zhang, X.-J., Runov, A., & Zelenyi, L. M. (2019). Ion anisotropy in Earth's magnetotail current sheet: Multicomponent ion population. *Journal of Geophysical Research: Space Physics*, *124*(5), 3454–3467. https://doi.org/10.1029/2019JA026604

Artemyev, A. V., Petrukovich, A. A., Nakamura, R., & Zelenyi, L. M. (2010). Proton velocity distribution in thin current sheets: Cluster observations and theory of transient trajectories. *Journal of Geophysical Research*, *115*(A12), A12255. https://doi.org/10.1029/2010JA015702

Artemyev, A. V., Petrukovich, A. A., Nakamura, R., & Zelenyi, L. M. (2011). Cluster statistics of thin current sheets in the Earth magnetotail: Specifics of the dawn flank, proton temperature profiles and electrostatic effects. *Journal of Geophysical Research*, *116*(A9), A09233. https://doi.org/10.1029/2011JA016801

Asano, Y., Nakamura, R., Baumjohann, W., Runov, A., Vörös, Z., Volwerk, M., et al. (2005). How typical are atypical current sheets? *Geophysical Research Letters*, *32*(3), L03108. https://doi.org/10.1029/2004GL021834

Baker, D. N., Pulkkinen, T. I., Angelopoulos, V., Baumjohann, W., & McPherron, R. L. (1996). Neutral line model of substorms: Past results and present view. *Journal of Geophysical Research*, *101*(A6), 12975–13010. https://doi.org/10.1029/95JA03753

Baumjohann, W., Roux, A., Le Contel, O., Nakamura, R., Birn, J., Hoshino, M., et al. (2007). Dynamics of thin current sheets: Cluster observations. *Annales Geophysicae*, *25*(6), 1365–1389. https://doi.org/10.5194/angeo-25-1365-2007

Biskamp, D. (1971). Instability of two-dimensional collisionless plasmas with neutral points. *Plasma Physics*, *13*(11), 1013–1026. https://doi.org/10.1088/0032-1028/13/11/003

Borg, A. L., Øieroset, M., Phan, T. D., Mozer, F. S., Pedersen, A., Mouikis, C., et al. (2005). Cluster encounter of a magnetic reconnection diffusion region in the near-Earth magnetotail on September 19, 2003. *Geophysical Research Letters*, *32*(19), L19105. https://doi.org/10.1029/2005GL023794

Burch, J. L., Moore, T. E., Torbert, R. B., & Giles, B. L. (2016). Magnetospheric multiscale overview and science objectives. *Space Science Reviews*, *199*(1), 5–21. https://doi.org/10.1007/s11214-015-0164-9

Dunlop, M. W., Balogh, A., Glassmeier, K.-H., & Robert, P. (2002). Four-point Cluster application of magnetic field analysis tools: The Curlometer. *Journal of Geophysical Research*, *107*(A11). SMP 23-1–SMP 23-14. https://doi.org/10.1029/2001JA005088

Eastwood, J. P., Phan, T.-D., Mozer, F. S., Shay, M. A., Fujimoto, M., Retinò, A., et al. (2007). Multi-point observations of the Hall electromagnetic field and secondary island formation during magnetic reconnection. *Journal of Geophysical Research*, *112*(A6), A06235. https://doi.org/10.1029/2006JA012158

Eastwood, J. P., Phan, T. D., Øieroset, M., & Shay, M. A. (2010). Average properties of the magnetic reconnection ion diffusion region in the Earth's magnetotail: The 2001–2005 Cluster observations and comparison with simulations. *Journal of Geophysical Research*, *115*(A8), A08215. https://doi.org/10.1029/2009JA014962

Ergun, R. E., Tucker, S., Westfall, J., Goodrich, K. A., Malaspina, D. M., Summers, D., et al. (2016). The axial double probe and fields signal processing for the MMS mission. *Space Science Reviews*, *199*(1), 167–188. https://doi.org/10.1007/s11214-014-0115-x

Fujimoto, M., Terasawa, T., Mukai, T., Saito, Y., Yamamoto, T., & Kokubun, S. (1998). Plasma entry from the flanks of the near-Earth magnetotail: Geotail observations. *Journal of Geophysical Research*, *103*(A3), 4391–4408. https://doi.org/10.1029/97JA03340

Genestreti, K. J., Farrugia, C. J., Lu, S., Vines, S. K., Reiff, P. H., Phan, T., et al. (2023a). Multiscale observation of magnetotail reconnection onset: 1. Macroscopic dynamics. *Journal of Geophysical Research: Space Physics*, *128*(11), e2023JA031758. https://doi.org/10.1029/2023JA031758

Genestreti, K. J., Farrugia, C. J., Lu, S., Vines, S. K., Reiff, P. H., Phan, T., et al. (2023b). Multi-scale observation of magnetotail reconnection onset: 2. Microscopic dynamics. *Journal of Geophysical Research: Space Physics*, *128*(11), e2023JA031760. https://doi.org/10.1029/2023JA031760

Harris, E. G. (1962). On a plasma sheath separating regions of oppositely directed magnetic field. *Il Nuovo Cimento - B*, *23*(1), 115–121. https://doi.org/10.1007/BF02733547

Hesse, M., Schindler, K., Birn, J., & Kuznetsova, M. (1999). The diffusion region in collisionless magnetic reconnection. *Physics of Plasmas*, *6*(5), 1781–1795. https://doi.org/10.1063/1.873436

Hesse, M., Winske, D., & Birn, J. (1998). On the ion-scale structure of thin current sheets in the magnetotail. *Physica Scripta*, *T74*, 63–66. https://doi.org/10.1088/0031-8949/1998/T74/012

Lindqvist, P.-A., Olsson, G., Torbert, R. B., King, B., Granoff, M., Rau, D., et al. (2016). The spin-plane double probe electric field instrument for MMS. *Space Science Reviews*, *199*(1), 137–165. https://doi.org/10.1007/s11214-014-0116-9

Lu, Q., Fu, H., Wang, R., & Lu, S. (2022). Collisionless magnetic reconnection in the magnetosphere. *Chinese Physics B*, *31*(8), 089401. https://doi.org/10.1088/1674-1056/ac76ab

Lu, S., Artemyev, A. V., Angelopoulos, V., Lin, Y., Zhang, X.-J., Liu, J., et al. (2019). The Hall electric field in Earth's magnetotail thin current sheet. *Journal of Geophysical Research: Space Physics*, *124*(2), 1052–1062. https://doi.org/10.1029/2018JA026202

Lu, S., Lin, Y., Angelopoulos, V., Artemyev, A. V., Pritchett, P. L., Lu, Q., & Wang, X. Y. (2016). Hall effect control of magnetotail dawn-dusk asymmetry: A three-dimensional global hybrid simulation. *Journal of Geophysical Research: Space Physics*, *121*(12), 11882–11895. https://doi.org/10.1002/2016JA023325

Lu, S., Lu, Q. M., Wang, R. S., Pritchett, P. L., Hubbert, M., Qi, Y., et al. (2022). Electron-only reconnection as a transition from quiet current sheet to standard reconnection in Earth's magnetotail: Particle-in-cell simulation and application to MMS data. *Geophysical Research Letters*, *49*(11), e2022GL098547. https://doi.org/10.1029/2022GL098547

Lu, S., Pritchett, P. L., Angelopoulos, V., & Artemyev, A. V. (2018). Formation of dawn-dusk asymmetry in Earth's magnetotail thin current sheet: A three-dimensional particle-in-cell simulation. *Journal of Geophysical Research: Space Physics*, *123*(4), 2801–2814. https://doi.org/10.1002/2017JA025095

Lu, S., Wang, R., Lu, Q., Angelopoulos, V., Nakamura, R., Artemyev, A. V., et al. (2020). Magnetotail reconnection onset caused by electron kinetics with a strong external driver. *Nature Communications*, *11*(1), 5049. https://doi.org/10.1038/s41467-020-18787-w

McPherron, R. L., Russell, C. T., & Aubry, M. P. (1973). Satellite studies of magnetospheric substorms on August 15, 1968: 9. Phenomenological model for substorms. *Journal of Geophysical Research*, *78*(16), 3131–3149. https://doi.org/10.1029/JA078i016p03131

Mitchell, D. G., Williams, D. J., Huang, C. Y., Frank, L. A., & Russell, C. T. (1990). Current carriers in the near-Earth cross-tail current sheet during substorm growth phase. *Geophysical Research Letters*, *17*(5), 583–586. https://doi.org/10.1029/GL017i005p00583

Øieroset, M., Phan, T. D., Fujimoto, M., Lin, R. P., & Lepping, R. P. (2001). In situ detection of collisionless reconnection in the Earth's magnetotail. *Nature*, *412*(6845), 414–417. https://doi.org/10.1038/35086520

Petrukovich, A., Artemyev, A., Vasko, I., Nakamura, R., & Zelenyi, L. (2015). Current sheets in the Earth magnetotail: Plasma and magnetic field structure with cluster project observations. *Space Science Reviews*, *188*(1), 311–337. https://doi.org/10.1007/s11214-014-0126-7

Petrukovich, A. A., Artemyev, A. V., Malova, H. V., Popov, V. Y., Nakamura, R., & Zelenyi, L. M. (2011). Embedded current sheets in the Earth's magnetotail. *Journal of Geophysical Research*, *116*(A5), A00I25. https://doi.org/10.1029/2010JA015749

Petrukovich, A. A., Baumjohann, W., Nakamura, R., & Runov, A. (2008). Formation of current density profile in tilted current sheets. *Annales Geophysicae*, *26*(12), 3669–3676. https://doi.org/10.5194/angeo-26-3669-2008

Pollock, C., Moore, T., Jacques, A., Burch, J., Gliese, U., Saito, Y., et al. (2017). Fast plasma investigation for magnetospheric multiscale (pp. 329–404). https://doi.org/10.1007/978-94-024-0861-4_12

Pritchett, P. L., & Coroniti, F. V. (1994). Convection and the formation of thin current sheets in the near-Earth plasma sheet. *Geophysical Research Letters*, *21*(15), 1587–1590. https://doi.org/10.1029/94GL01364

Pritchett, P. L., & Lu, S. (2018). Externally driven onset of localized magnetic reconnection and disruption in a magnetotail configuration. *Journal of Geophysical Research: Space Physics*, *123*(4), 2787–2800. https://doi.org/10.1002/2017JA025094

Pulkkinen, T. I., Baker, D. N., Cogger, L. L., Frank, L. A., Sigwarth, J. B., Kokubun, S., et al. (1999). Spatial extent and dynamics of a thin current sheet during the substorm growth phase on December 10, 1996. *Journal of Geophysical Research*, *104*(A12), 28475–28490. https://doi.org/10.1029/1999JA900240

Rich, F. J., Vasyliunas, V. M., & Wolf, R. A. (1972). On the balance of stresses in the plasma sheet. *Journal of Geophysical Research*, *77*(25), 4670–4676. https://doi.org/10.1029/JA077i025p04670

Rogers, A. J., Farrugia, C. J., Torbert, R. B., & Rogers, T. J. (2023). Applying magnetic curvature to MMS data to identify thin current sheets relative to tail reconnection. *Journal of Geophysical Research: Space Physics*, *128*(1), e2022JA030577. https://doi.org/10.1029/2022JA030577

Rong, Z. J., Shen, C., Petrukovich, A. A., Wan, W. X., & Liu, Z. X. (2010). The analytic properties of the flapping current sheets in the earth magnetotail. *Planetary and Space Science*, *58*(10), 1215–1229. https://doi.org/10.1016/j.pss.2010.04.016

Rong, Z. J., Wan, W. X., Shen, C., Li, X., Dunlop, M. W., Petrukovich, A. A., et al. (2011). Statistical survey on the magnetic structure in magnetotail current sheets. *Journal of Geophysical Research*, *116*(A9), A09218. https://doi.org/10.1029/2011JA016489

Runov, A., Angelopoulos, V., Artemyev, A. V., Weygand, J. M., Lu, S., Lin, Y., & Zhang, X.-J. (2021). Global and local processes of thin current sheet formation during substorm growth phase. *Journal of Atmospheric and Solar-Terrestrial Physics*, *220*, 105671. https://doi.org/10.1016/j.jastp.2021.105671

Runov, A., Sergeev, V. A., Baumjohann, W., Nakamura, R., Apatenkov, S., Asano, Y., et al. (2005). Electric current and magnetic field geometry in flapping magnetotail current sheets. *Annales Geophysicae*, *23*(4), 1391–1403. https://doi.org/10.5194/angeo-23-1391-2005

Runov, A., Sergeev, V. A., Nakamura, R., Baumjohann, W., Apatenkov, S., Asano, Y., et al. (2006). Local structure of the magnetotail current sheet: 2001 Cluster observations. *Annales Geophysicae*, *24*(1), 247–262. https://doi.org/10.5194/angeo-24-247-2006

Runov, A., Sergeev, V. A., Nakamura, R., Baumjohann, W., Zhang, T. L., Asano, Y., et al. (2005). Reconstruction of the magnetotail current sheet structure using multi-point Cluster measurements. *Planetary and Space Science*, *53*(1–3), 237–243. https://doi.org/10.1016/j.pss.2004.09.049

Russell, C. T., Anderson, B. J., Baumjohann, W., Bromund, K. R., Dearborn, D., Fischer, D., et al. (2016). The magnetospheric multiscale magnetometers. *Space Science Reviews*, *199*(1), 189–256. https://doi.org/10.1007/s11214-014-0057-3

Sanny, J., McPherron, R. L., Russell, C. T., Baker, D. N., Pulkkinen, T. I., & Nishida, A. (1994). Growth-phase thinning of the near-Earth current sheet during the CDAW 6 substorm. *Journal of Geophysical Research*, *99*(A4), 5805–5816. https://doi.org/10.1029/93JA03235

Sergeev, V., Angelopoulos, V., Carlson, C., & Sutcliffe, P. (1998). Current sheet measurements within a flapping plasma sheet. *Journal of Geophysical Research*, *103*(A5), 9177–9187. https://doi.org/10.1029/97JA02093

Sergeev, V. A., Mitchell, D. G., Russell, C. T., & Williams, D. J. (1993). Structure of the tail plasma/current sheet at ∼11 R_E and its changes in the course of a substorm. *Journal of Geophysical Research*, *98*(A10), 17345–17365. https://doi.org/10.1029/93JA01151

Sergeev, V. A., Sormakov, D. A., Apatenkov, S. V., Baumjohann, W., Nakamura, R., Runov, A. V., et al. (2006). Survey of large-amplitude flapping motions in the midtail current sheet. *Annales Geophysicae*, *24*(7), 2015–2024. https://doi.org/10.5194/angeo-24-2015-2006

Shukhtina, M. A., Dmitrieva, N. P., & Sergeev, V. A. (2004). Quantitative magnetotail characteristics of different magnetospheric states. *Annales Geophysicae*, *22*(3), 1019–1032. https://doi.org/10.5194/angeo-22-1019-2004

Sitnov, M., Birn, J., Ferdousi, B., Gordeev, E., Khotyaintsev, Y., Merkin, V., et al. (2019). Explosive magnetotail activity. *Space Science Reviews*, *215*(4), 31. https://doi.org/10.1007/s11214-019-0599-5

Sitnov, M. I., & Arnold, H. (2022). Equilibrium kinetic theory of weakly anisotropic embedded thin current sheets. *Journal of Geophysical Research: Space Physics*, *127*(11), e2022JA030945. https://doi.org/10.1029/2022JA030945

Sitnov, M. I., & Merkin, V. G. (2016). Generalized magnetotail equilibria: Effects of the dipole field, thin current sheets, and magnetic flux accumulation. *Journal of Geophysical Research: Space Physics*, *121*(8), 7664–7683. https://doi.org/10.1002/2016JA023001

Sitnov, M. I., Stephens, G. K., Tsyganenko, N. A., Miyashita, Y., Merkin, V. G., Motoba, T., et al. (2019). Signatures of nonideal plasma evolution during substorms obtained by mining multimission magnetometer data. *Journal of Geophysical Research: Space Physics*, *124*(11), 8427–8456. https://doi.org/10.1029/2019JA027037

Sitnov, M. I., Swisdak, M., Guzdar, P. N., & Runov, A. (2006). Structure and dynamics of a new class of thin current sheets. *Journal of Geophysical Research*, *111*(A8), A08204. https://doi.org/10.1029/2005JA011517

Sonnerup, B. U. O., & Scheible, M. P. (1998). Minimum and maximum variance analysis. Retrieved from https://api.semanticscholar.org/CorpusID:118577335

Torbert, R. B., Russell, C. T., Magnes, W., Ergun, R. E., Lindqvist, P.-A., LeContel, O., et al. (2016). The FIELDS Instrument Suite on MMS: Scientific objectives, measurements, and data products. *Space Science Reviews*, *199*(1), 105–135. https://doi.org/10.1007/s11214-014-0109-8

Tsai, E., Artemyev, A. V., & Angelopoulos, V. (2017). Ion motion in a polarized current sheet. *Physics of Plasmas*, *24*(1), 012908. https://doi.org/10.1063/1.4975017

Vasko, I. Y., Petrukovich, A. A., Artemyev, A. V., Nakamura, R., & Zelenyi, L. M. (2015). Earth's distant magnetotail current sheet near and beyond lunar orbit. *Journal of Geophysical Research: Space Physics*, *120*(10), 8663–8680. https://doi.org/10.1002/2015JA021633

Yoon, P. H., & Lui, A. T. Y. (2005). A class of exact two-dimensional kinetic current sheet equilibria. *Journal of Geophysical Research*, *110*(A1), A01202. https://doi.org/10.1029/2003JA010308

Young, D. T., Burch, J. L., Gomez, R. G., De Los Santos, A., Miller, G. P., Wilson, P., et al. (2016). Hot plasma composition analyzer for the magnetospheric multiscale mission. *Space Science Reviews*, *199*(1), 407–470. https://doi.org/10.1007/s11214-014-0119-6

Zelenyi, L. M., Malova, H. V., Artemyev, A. V., Popov, V. Y., & Petrukovich, A. A. (2011). Thin current sheets in collisionless plasma: Equilibrium structure, plasma instabilities, and particle acceleration. *Plasma Physics Reports*, *37*(2), 118–160. https://doi.org/10.1134/S1063780X1102005X